Proceedings of the IEEE International Conference on Robotics and Automation, April 21-27 1997, Albuquerque, NM.

On the Control of Space Free-Flyers Using Multiple Impedance Control

S. Ali A. Moosavian, Evangelos Papadopoulos

Department of Mechanical Engineering & Centre for Intelligent Machines
McGill University
Montreal, Quebec, Canada H3A 2A7

Abstract. *The Multiple Impedance Control (MIC) is a new algorithm which enforces a designated impedance on both a manipulated object, and all cooperating manipulators. In this paper, the MIC is applied to a space robotic system in which robotic arms, mounted on a free-flying-base, manipulate an object. The general formulation of the MIC is extended to include the dynamic coupling between the arms and the base. It is shown that under the MIC law, all participating manipulators, the free-flyer base, and the manipulated object exhibit the same designated impedance behavior. This guarantees good tracking of system manipulators and the object, in performing a manipulation task. A system of two cooperating two-link manipulators is simulated, in which a Remote Centre Compliance is attached to the second end-effector. The object is grabbed with a pivoted grasp condition, i.e. both the translational and rotational motions of the object have to be controlled by end-effector forces. As simulation results show, the response of the MIC algorithm is smooth, even in the occurrence of an impact due to collision with an obstacle.*

I. Introduction.

Free-flying space manipulator systems, in which robotic manipulators are mounted on a free-flying spacecraft, are envisioned for assembling, maintenance, repair, and contingency operations in space. Early research work in this area focused on the dynamics and motion control of a single manipulator in free-floating mode [1]-[4], i.e. an end-effector moves toward a target in the inertial or spacecraft body-fixed frame with no significant force interactions between the system and the environment. Dynamics and motion control of multiple manipulators in both free-floating and free-flying modes have been studied by various researchers recently [5]-[7]. However, coordination and control of the spacecraft and its multiple manipulators during capture or manipulation of objects has not attracted adequate attention. These tasks require employing force or impedance control strategies, so that interaction forces and system response during contact are controlled.

As an extension of Hogan's impedance control concept [8], the *Object Impedance Control* (OIC) has been developed for multiple robotic arms manipulating a common object [9]. A combination of feedforward and feedback control is employed to make the object behave like a reference impedance. However, it has been realized that applying the OIC to manipulation of a flexible object may lead to instability [10]. Based on the analysis of a representative system, it was suggested that in order to solve the instability problem, one should either increase the desired mass parameters or filter and lower the frequency content of the estimated contact force.

In a recent study, a new algorithm named as *Multiple Impedance Control* (MIC) was developed which enforces a designated impedance of both manipulator end-points, *and* of a manipulated object [11]. Physically speaking, this means that all participating end-effectors and the manipulated object are controlled to behave like a designated impedance in reaction to any disturbing external force on the object. This results in good tracking of the various manipulators of the system and the object. The MIC algorithm is able to perform both free motions and contact tasks without switching between control modes. In addition, object inertia effects are compensated for in the impedance law, and the end-effector(s) tracking errors are controlled.

In this paper, the new MIC algorithm is applied to space robotic systems in which manipulators are mounted on a free-flying base. The general formulation is adapted to consider the dynamic coupling between the arms and the base while the manipulated object may include an internal source of angular momentum. Next, it is shown by error

analysis that under the MIC law all participating manipulators, the free-flyer base, and the manipulated object exhibit the same designated impedance behavior. Finally, a system of two cooperating two-link manipulators is simulated, and the obtained results are discussed.

II. The MIC Law for Space Free-Flyers.

When applied to a terrestrial system, the MIC strategy enforces the same impedance relationship at the manipulator end-effector level, *and* at the manipulated object level. In space, since the cooperating robotic arms are connected through a free-flying base, the MIC algorithm is applied so that all participating manipulators, the spacecraft, and the manipulated object exhibit the same impedance behavior, as implied by "multiple" in naming the MIC. This strategy allows coordinated motion/force control of the space free-flying robot for performing a manipulation task. In this section, following a brief review on space free-flyers and object dynamics, the MIC law for space applications is presented.

(a) System Dynamics Modelling. The vector of generalized coordinates for a space free-flyer with multiple manipulators, shown in Figure 1, can be chosen as

$$\mathbf{q} = (\mathbf{R}_{C_0}^T, \boldsymbol{\delta}_0^T, \boldsymbol{\theta}^T)^T \tag{1}$$

where $\mathbf{R}_{C_0}$ describes the inertial position of the spacecraft center of mass (CM), $\boldsymbol{\delta}_0$ is a set of Euler angles that describes the orientation of the spacecraft, and $\boldsymbol{\theta} = \left(\boldsymbol{\theta}^{(1)T}, \boldsymbol{\theta}^{(2)T}, \cdots, \boldsymbol{\theta}^{(n)T}\right)^T$ is a K×1 column vector which contains all joint angle vectors. The $\boldsymbol{\theta}^{(m)}$ is an $N_m \times 1$ column vector which contains the joint angles of the m-th manipulator, and $K = \sum_{m=1}^{n} N_m$. Assuming that the system consists of rigid elements and applying the general Lagrangian formulation, the equations of motion can be obtained as [12]-[13]

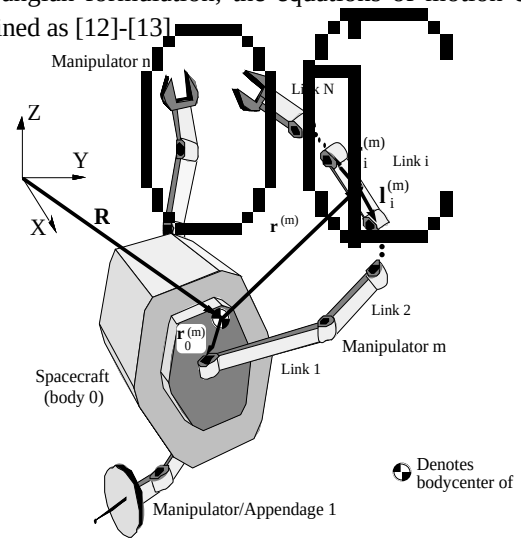

Fig. 1: A space free-flyer with n manipulators.

$$\mathbf{H}(\boldsymbol{\delta}_0, \boldsymbol{\theta})\ddot{\mathbf{q}} + \mathbf{C}(\boldsymbol{\delta}_0, \dot{\boldsymbol{\delta}}_0, \boldsymbol{\theta}, \dot{\boldsymbol{\theta}}) = \mathbf{Q}(\boldsymbol{\delta}_0, \boldsymbol{\theta}) \tag{2}$$

where $\mathbf{H}$ is an N×N positive definite mass matrix of the system ($N = K + 6$ is the total system degree of freedom), $\mathbf{C}$ is an N×1 vector which contains all the nonlinear velocity terms (in a microgravity environment), and $\mathbf{Q}$ is the N×1 vector of generalized forces.

The vector of output (controlled) variables is defined as

$$\tilde{\mathbf{x}} = [\mathbf{R}_{C_0}^T, \boldsymbol{\delta}_0^T, \mathbf{x}_E^{(1)T}, \boldsymbol{\delta}_E^{(1)T}, \cdots, \mathbf{x}_E^{(n)T}, \boldsymbol{\delta}_E^{(n)T}]^T \tag{3}$$

where $\mathbf{x}_E^{(m)}$ describes the m-th end-effector inertial position, and $\boldsymbol{\delta}_E^{(m)}$ is a set of Euler angles which describes the m-th end-effector orientation. It is assumed that all manipulators have six DOF, i.e. $K = 6n$ (n is the number of participating manipulators), and that they all participate in manipulating the object. The vector of output speeds $\dot{\tilde{\mathbf{x}}}$ is obtained from the time derivative of the generalized coordinates ($\dot{\mathbf{q}}$), using a square Jacobian $\mathbf{J}_C$

$$\dot{\tilde{\mathbf{x}}} = \mathbf{J}_C \dot{\mathbf{q}} \tag{4}$$

The equations of motion can now be written in the task space, i.e. in terms of the output coordinates $\tilde{\mathbf{x}}$, as

$$\tilde{\mathbf{H}}(\mathbf{q})\ddot{\tilde{\mathbf{x}}} + \tilde{\mathbf{C}}(\mathbf{q}, \dot{\mathbf{q}}) = \tilde{\mathbf{Q}} \tag{5a}$$

where

$$\tilde{\mathbf{H}} = \mathbf{J}_C^{-T}\,\mathbf{H}\,\mathbf{J}_C^{-1} \qquad \tilde{\mathbf{C}} = \mathbf{J}_C^{-T}\mathbf{C} - \tilde{\mathbf{H}}\dot{\mathbf{J}}_C\dot{\mathbf{q}} \qquad \tilde{\mathbf{Q}} = \mathbf{J}_C^{-T}\mathbf{Q} \tag{5b}$$

To develop the MIC law, the vector of generalized forces in the task space, $\tilde{\mathbf{Q}}$, is written as

$$\tilde{\mathbf{Q}} = \tilde{\mathbf{Q}}_{app} + \tilde{\mathbf{Q}}_{react} = \tilde{\mathbf{Q}}_m + \tilde{\mathbf{Q}}_f + \tilde{\mathbf{Q}}_{react} \tag{6}$$

where $\tilde{\mathbf{Q}}_{react}$ is the reaction force on the end-effectors, and $\tilde{\mathbf{Q}}_{app}$ is the applied controlling force consisting of the force which corresponds to the motion of the system, $\tilde{\mathbf{Q}}_m$, and of the required force to be applied on the manipulated object by the end-effectors, $\tilde{\mathbf{Q}}_f$. These terms will be detailed after describing object dynamics.

(b) Object Dynamics. The equations of motion for the object can be written based on rigid-body dynamics. For a flexible object an appropriate dynamics model can be simply substituted for the following model. Also, the object may include an internal angular momentum source, see Figure 2. Thus, the object dynamics can be expressed as

$$\mathbf{M}\ddot{\mathbf{x}} + \mathbf{F}_\omega = \mathbf{F}_c + \mathbf{F}_o + \mathbf{G}\mathbf{F}_e \tag{7}$$

where $\mathbf{M}$ is the mass matrix, $\mathbf{x} = (\mathbf{x}_G^T, \boldsymbol{\delta}_{obj}^T)^T$ describes the position of the object center of mass $\mathbf{x}_G$ and the object orientation described by Euler angles $\boldsymbol{\delta}_{obj}$, $\mathbf{F}_\omega$ is a vector of nonlinear velocity terms, $\mathbf{F}_c$ describes the contact forces/moments, $\mathbf{F}_o$ describes external forces/torques (other than contact and end-effector ones), $\mathbf{F}_e$ is a $6n \times 1$ vector

which contains all end-effector forces/torques applied on the object ($\mathbf{F}_e^{(i)}$ is a 6×1 vector corresponding to the i-th end-effector), and the matrix $\mathbf{G}$ is referred to as the grasp matrix, [11]. Next, using the system dynamics model and the object dynamics equations, the MIC law for space applications is developed.

(c) The Control Law. A desired impedance law for the object motion can be chosen as

$$\mathbf{M}_{des}\ddot{\mathbf{e}} + \mathbf{k}_d\dot{\mathbf{e}} + \mathbf{k}_p\mathbf{e} + \mathbf{F}_c = \mathbf{0} \tag{8}$$

where $\mathbf{e} = (\mathbf{x}_{des} - \mathbf{x})$ describes the object tracking error, $\mathbf{k}_p$ and $\mathbf{k}_d$ are control gain matrices, and $\mathbf{M}_{des}$ is the object desired mass matrix. Then, by direct comparison of Eq. (8) and Eq. (7), it can be seen that the desired impedance behavior can be obtained if

$$\begin{aligned}\mathbf{G}\mathbf{F}_{e_{req}} = \mathbf{M}\mathbf{M}_{des}^{-1}\left(\mathbf{M}_{des}\ddot{\mathbf{x}}_{des} + \mathbf{k}_d\dot{\mathbf{e}} + \mathbf{k}_p\mathbf{e} + \mathbf{F}_c\right) + \\ \mathbf{F}_\omega - \left(\mathbf{F}_c + \mathbf{F}_o\right)\end{aligned} \tag{9}$$

provided that the matrix $\mathbf{S}_{obj}$ which relates the object angular velocity, $\boldsymbol{\omega}_{obj}$, to the Euler rates, $\dot{\boldsymbol{\delta}}_{obj}$, as [14]

$$\boldsymbol{\omega}_{obj} = \mathbf{S}_{obj}\,\dot{\boldsymbol{\delta}}_{obj} \tag{10}$$

is not singular. Clearly, this depends on the Euler angles definition. Therefore, applying the required end-effector forces/torques on the object, $\mathbf{F}_{e_{req}}$, results in the targeted impedance relationship as described in Eq. (8). Eq. (9) can be solved to obtain a minimum norm solution, resulting in

$$\begin{aligned}\mathbf{F}_{e_{req}} = \mathbf{G}^{\#}\{\mathbf{M}\mathbf{M}_{des}^{-1}\left(\mathbf{M}_{des}\ddot{\mathbf{x}}_{des} + \mathbf{k}_d\dot{\mathbf{e}} + \mathbf{k}_p\mathbf{e} + \hat{\mathbf{F}}_c\right) + \\ \mathbf{F}_\omega - \left(\hat{\mathbf{F}}_c + \mathbf{F}_o\right)\}\end{aligned} \tag{11}$$

where $\mathbf{G}^{\#}$ is the pseudoinverse of the grasp matrix, a full-rank matrix (provided that $\mathbf{S}_{obj}$ is not singular) defined as

$$\mathbf{G}^{\#} = \mathbf{W}^{-1}\mathbf{G}^T\left(\mathbf{G}\mathbf{W}^{-1}\mathbf{G}^T\right)^{-1} \tag{12}$$

weighted by a task weighting matrix $\mathbf{W}$, so that linear and angular motions or their components are weighted appropriately. Note that $\hat{\mathbf{F}}_c$ is the estimated value of the contact force $\mathbf{F}_c$ which can be computed as [11]

$$\hat{\mathbf{F}}_c = \mathbf{M}\ddot{\hat{\mathbf{x}}} + \mathbf{F}_\omega - \mathbf{F}_o - \mathbf{G}\mathbf{F}_e \tag{13}$$

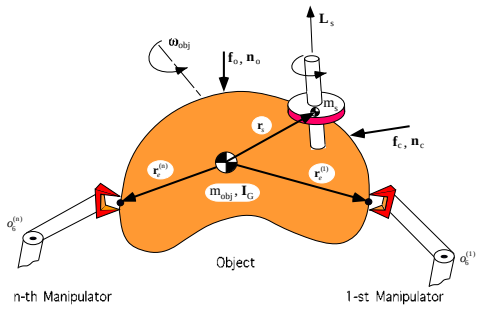

Fig. 2: An object with an internal angular momentum source, manipulated by a multiple arm free-flying robot.

with

$$\ddot{\hat{\mathbf{x}}} = \frac{\dot{\mathbf{x}}_t - \dot{\mathbf{x}}_{t-\Delta t}}{\Delta t} \quad \text{or} \quad \ddot{\hat{\mathbf{x}}} = \frac{\mathbf{x}_t - 2\mathbf{x}_{t-\Delta t} + \mathbf{x}_{t-2\Delta t}}{(\Delta t)^2} \tag{14}$$

where Δt is the time step used in the estimation procedure. In a noisy environment higher order finite difference estimates may be needed. Note that due to practical reasons (i.e. time requirement for measurements and corresponding calculations), Δt can not be infinitesimally close to zero. At sufficiently high sampling rates, this does not introduce a significant error, even during contact.

If, based on the grasp condition, it is required to apply additional internal forces and moments on the object, $\mathbf{F}_{\text{int}}$, then, Eq. (12) can be modified to

$$\begin{aligned}\mathbf{F}_{e_{req}} = \mathbf{G}^{\#}\{\mathbf{M}\mathbf{M}_{des}^{-1}\left(\mathbf{M}_{des}\ddot{\mathbf{x}}_{des} + \mathbf{k}_d\dot{\mathbf{e}} + \mathbf{k}_p\mathbf{e} + \hat{\mathbf{F}}_c\right) + \\ \mathbf{F}_\omega - \left(\hat{\mathbf{F}}_c + \mathbf{F}_o\right)\} + \left(\mathbf{1} - \mathbf{G}^{\#}\mathbf{G}\right)\mathbf{F}_{\text{int}}\end{aligned} \tag{15}$$

where $\mathbf{1}$ is a $6n\times 6n$ identity matrix. It can be easily shown that since the added term is in the null space of the grasp matrix $\mathbf{G}$, $\mathbf{F}_{\text{int}}$ does not affect the object motion. However, in space operations it is expected that a targeted object will be grabbed with a special tool or grippers. In such cases, it is expected that internal forces and moments will be minimal and hence, $\mathbf{F}_{\text{int}}$ can be chosen equal to zero.

Based on the above, the controlled force $\tilde{\mathbf{Q}}_f$ in Eq. (6) required to be applied on the manipulated object by the end-effectors is

$$\tilde{\mathbf{Q}}_f = \begin{Bmatrix}\mathbf{0}_{6\times 1}\\ \mathbf{F}_{e_{req}}\end{Bmatrix} \tag{16}$$

and, the reaction force on the end-effectors is

$$\tilde{\mathbf{Q}}_{react} = \begin{Bmatrix}\mathbf{0}_{6\times 1}\\ -\mathbf{F}_e\end{Bmatrix} \tag{17a}$$

where

$$\mathbf{F}_e = \mathbf{G}^{\#}\left[\mathbf{M}\ddot{\mathbf{x}} + \mathbf{F}_\omega - (\mathbf{F}_c + \mathbf{F}_o)\right] \tag{17b}$$

Next, to complete the computation of the controlling force $\tilde{\mathbf{Q}}$ as described in Eq. (6), an expression for $\tilde{\mathbf{Q}}_m$ must be obtained. To impose the same impedance law on the spacecraft motion, manipulators, and the object, the impedance law for the space free-flyer is written as

$$\tilde{\mathbf{M}}_{des}\ddot{\tilde{\mathbf{e}}} + \tilde{\mathbf{k}}_d\dot{\tilde{\mathbf{e}}} + \tilde{\mathbf{k}}_p\tilde{\mathbf{e}} + \mathbf{U}_{f_c}\mathbf{F}_c = \mathbf{0}_{\mathrm{N}\times 1} \tag{18}$$

where $\tilde{\mathbf{e}} = \tilde{\mathbf{x}}_{des} - \tilde{\mathbf{x}}$ is the tracking error in the system controlled variables as opposed to $\mathbf{e}$ which describes the object tracking error, $\mathbf{U}_{f_c} = \left[\mathbf{1}_{6\times 6} \quad \cdots \quad \mathbf{1}_{6\times 6}\right]^T$ is an $\mathrm{N}\times 6$ matrix, and $\tilde{\mathbf{M}}_{des}$, $\tilde{\mathbf{k}}_d$, and $\tilde{\mathbf{k}}_p$ are $\mathrm{N}\times\mathrm{N}$ block-diagonal matrices defined based on $\mathbf{M}_{des}$, $\mathbf{k}_p$, and $\mathbf{k}_d$, respectively. The desired trajectory for the system controlled variables, $\tilde{\mathbf{x}}_{des}$, can be defined based on the desired trajectory for the object motion, $\mathbf{x}_{des}$, and the grasp condition. Then, similar

to the derivation for $\tilde{\mathbf{Q}}_f$ and assuming that the system mass and geometric parameters are known, $\tilde{\mathbf{Q}}_m$ can be obtained as

$$\tilde{\mathbf{Q}}_m = \tilde{\mathbf{H}}\tilde{\mathbf{M}}_{des}^{-1}\left[\tilde{\mathbf{M}}_{des}\ddot{\tilde{\mathbf{x}}}_{des} + \tilde{\mathbf{k}}_d\dot{\tilde{\mathbf{e}}} + \tilde{\mathbf{k}}_p\tilde{\mathbf{e}} + \mathbf{U}_{f_c}\hat{\mathbf{F}}_c\right] + \tilde{\mathbf{C}} \qquad (19)$$

where $\tilde{\mathbf{M}}_{des}^{-1}$ is the block-inverse of $\tilde{\mathbf{M}}_{des}$.

III. Error Analysis.

Substituting Eqs. (19), (17a), and (16) into Eq. (6), and the result into Eq. (5a) yields

$$\tilde{\mathbf{H}}\left(\tilde{\mathbf{M}}_{des}^{-1}\left(\tilde{\mathbf{M}}_{des}\ddot{\tilde{\mathbf{x}}}_{des} + \tilde{\mathbf{k}}_d\dot{\tilde{\mathbf{e}}} + \tilde{\mathbf{k}}_p\tilde{\mathbf{e}} + \mathbf{U}_{f_c}\mathbf{F}_c\right) - \ddot{\tilde{\mathbf{x}}}\right) + \left\{\begin{array}{c}\mathbf{0}_{6\times 1}\\ \mathbf{G}^{\#}\mathbf{M}\left(\mathbf{M}_{des}^{-1}\left(\mathbf{M}_{des}\ddot{\mathbf{x}}_{des} + \mathbf{k}_d\dot{\mathbf{e}} + \mathbf{k}_p\mathbf{e} + \mathbf{F}_c\right) - \ddot{\mathbf{x}}\right)\end{array}\right\} = \mathbf{0} \qquad (20)$$

where it is assumed that the exact value of the contact force is available, and that the mass and geometric properties for the manipulated object, and the space free-flying manipulator system are known. Since Eq. (20) must hold for any $\mathbf{M}$ and any $\tilde{\mathbf{H}}$, it is concluded that

$$\begin{aligned}&\tilde{\mathbf{H}}\left(\tilde{\mathbf{M}}_{des}^{-1}\left(\tilde{\mathbf{M}}_{des}\ddot{\tilde{\mathbf{x}}}_{des} + \tilde{\mathbf{k}}_d\dot{\tilde{\mathbf{e}}} + \tilde{\mathbf{k}}_p\tilde{\mathbf{e}} + \mathbf{U}_{f_c}\mathbf{F}_c\right) - \ddot{\tilde{\mathbf{x}}}\right) = \mathbf{0}\\ &\mathbf{G}^{\#}\mathbf{M}\left(\mathbf{M}_{des}^{-1}\left(\mathbf{M}_{des}\ddot{\mathbf{x}}_{des} + \mathbf{k}_d\dot{\mathbf{e}} + \mathbf{k}_p\mathbf{e} + \mathbf{F}_c\right) - \ddot{\mathbf{x}}\right) = \mathbf{0}\end{aligned} \qquad (21)$$

Since $\mathbf{G}^{\#}$ is of full-rank, and $\mathbf{M}$ and $\tilde{\mathbf{H}}$ are positive definite inertia matrices, Eq. (21) results in

$$\begin{aligned}&\tilde{\mathbf{M}}_{des}\ddot{\tilde{\mathbf{e}}} + \tilde{\mathbf{k}}_d\dot{\tilde{\mathbf{e}}} + \tilde{\mathbf{k}}_p\tilde{\mathbf{e}} + \mathbf{U}_{f_c}\mathbf{F}_c = \mathbf{0}\\ &\mathbf{M}_{des}\ddot{\mathbf{e}} + \mathbf{k}_d\dot{\mathbf{e}} + \mathbf{k}_p\mathbf{e} + \mathbf{F}_c = \mathbf{0}\end{aligned} \qquad (22)$$

Considering the definitions for $\tilde{\mathbf{M}}_{des}$, $\tilde{\mathbf{k}}_d$, $\tilde{\mathbf{k}}_p$, and $\mathbf{U}_{f_c}$, Eq. (22) means that all participating manipulators, the free-flyer-base, and the manipulated object exhibit the *same* impedance behavior. This guarantees an accordant motion of the various subsystems during object manipulation tasks.

IV. Simulation Results.

Task Definition. Figure 3 shows a robotic system in planar motion, performing a *cooperative manipulation task*, i.e. moving an object with two manipulators according to predefined trajectories. It is assumed that the position and attitude of the system base is controlled and does not move. One of the two end-effectors is equipped with a Remote Centre Compliance (RCC). The task is to move an object based on a given trajectory which for illustration purposes passes through an obstacle. The object has to come to a smooth stop at the obstacle. Initially, the object has been grabbed with a pivoted grasp condition, i.e. no torque can be exerted on the object by the two end-effectors. Therefore, both the translational and rotational motions of the object are controlled by end-effector *forces*.

Simulation Results and Discussions. For the system depicted in Figure 3, the geometric parameters, mass properties, and the maximum available actuator torques are displayed in Table 1. The origin of the inertial frame is considered to be located at joint 1 of the first manipulator, and joint 1 of the second manipulator is at $(1.2\text{ m}, 0.0)^{\mathrm{T}}$. The object and controller parameters are

$$m_{obj} = 3.0\ kg,\ I_G = 0.5\ kg\,m^2,\ {}^0\mathbf{r}_e^{(1)} = -{}^0\mathbf{r}_e^{(2)} = (-0.3, 0.0)\,m$$

$$\mathbf{M}_{des} = diag(10,10), \mathbf{k}_p = diag(100,100), \mathbf{k}_d = diag(300,300)$$

The initial conditions are

$$(q_1^{(1)}, q_2^{(1)}, \dot{q}_1^{(1)}, \dot{q}_2^{(1)}, q_1^{(2)}, q_2^{(2)}, \dot{q}_1^{(2)}, \dot{q}_2^{(2)}, \theta, \dot{\theta})^T = (2.7, -2.7, 0, 0, 1.0, 2.5, 0, 0, 0, 0)^T \quad (rad, rad/s)$$

It is assumed that the RCC unit is initially free of tension or compression, where its stiffness and damping properties are chosen as $\mathbf{k}_e = diag(2,2)\times 10^4\ kg/\sec^2$, and $\mathbf{b}_e = diag(5,5)\times 10^2\ kg/\sec$, see [15].

The desired trajectory for the object center of mass, expressed in the inertial frame, is

$$x_{G\,des} = 1 - e^{-t}\ m,\ y_{G\,des} = 0.5\ m,\ \theta_{des} = \theta_0$$

Table 1: The system Parameters.

Manipulator	i-th body	${}^i\mathbf{r}_i$ (m) (m)	${}^i\mathbf{l}_i$ (m) (m)	m_i (m) (kg)	I_i (m) (kgm^2)	τ_i (m) (N-m)
1	1	0,0.50	0,-0.50	10.0	1.50	100.0
1	2	0,0.50	0,-0.50	6.0	0.80	100.0
2	1	0,0.50	0,-0.50	10.0	1.50	100.0
2	2	0,0.50	0,-0.50	8.0	0.80	100.0

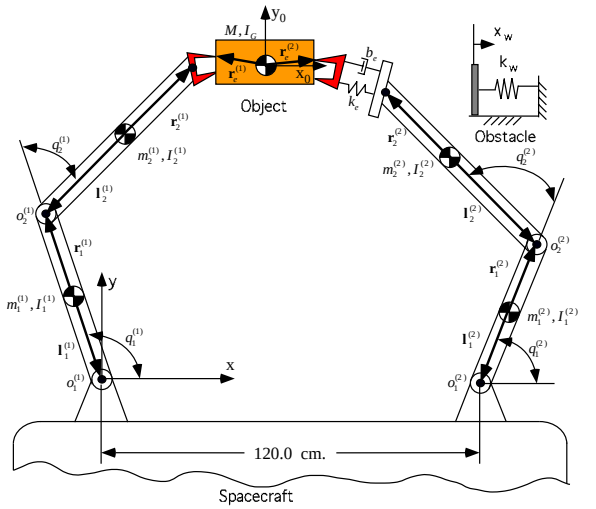

Fig. 3: Two robotic arms mounted on a spacecraft, performing a cooperative manipulation task on a plane.

where θ_0 describes the object initial orientation. The obstacle is at $x_w = 1.2\ m$, so it is expected that the object

will come in contact at its right side, i.e. at $\mathbf{x}_G + \mathbf{r}_e^{(2)}$. It is assumed that no torque is developed at the contact surface (i.e. a *point contact* occurs), therefore $\mathbf{n}_c$ is equal to the moment of $\mathbf{f}_c$. Also, there is no other external force applied on the object, i.e. $\mathbf{f}_o = \mathbf{0}, \mathbf{n}_o = \mathbf{0}$. The contact force is estimated based on Eqs. (13, 14b), where the real stiffness of the obstacle is $k_w = 1e5\ N/m$. The time step, Δt, in the estimation procedure (Eq. (14)) is 10 msec. Given the above information, the obtained simulation results are presented in Figure 4.

As shown in Figures 4a,b the y-component of the error in the object position, starting from some initial value, converges to zero smoothly. This is due to the fact that contact occurs along the x-direction, and so the contact force does not affect the object's motion in the y-direction. The x-component of the error, decreases at some rate until contact occurs at $t \approx 1.0$ sec. This rate changes after contact, because the error dynamics depend on the dynamics of the environment, according to the impedance law. Then, this error smoothly converges to the distance between the final desired x-position and the obstacle x-position.

The object orientation error, starting from zero, grows to some amount and then converges to zero, Figure 4a. The initial growth is due to the fact that the first end-effector (i.e. without the RCC unit) responds faster than the second one which is equipped with the RCC. Therefore, the difference between the two end-effector forces produces some moments which results in an undesirable rotation of the object. However, after a short transient period the difference vanishes and so does the object orientation error.

Actuator saturation limits are reached at start-up (because of large initial errors and error-rates), and at the time of contact, Figures 4c,d. Joint torques for the first manipulator converge to a steady state soon after contact (about half of a second), while it takes longer for those of the second manipulator. Again, this is due to the existence of the RCC.

The contact with the obstacle occurs along the x-direction when the right end of the object goes beyond x_W. Therefore, f_{c_y} remains equal to zero before and after contact, while f_{c_x} appears whenever the object is in contact with the obstacle, Figure 4e. As the impact energy is dissipated, f_{c_x} converges to a constant value. According to the imposed impedance law, Eq. (8), for diagonal gain matrices this constant force has to be equal to $-k_p e_x = -100(0.1) = -10\ N$, which is verified from the response results. Figure 4f shows the difference between the real value of the contact force, and the estimated one used by the controller. As can be seen, the difference is almost zero except during a very short period following impact. Even then, the difference is quite small (about 10% of the real value). After this period, the acceleration profiles become smoother and the difference between the real and estimated values of the contact force becomes zero. Note that before the contact, the slight difference between the two is due to the approximation of object acceleration, based on calculation of Eq. (14).

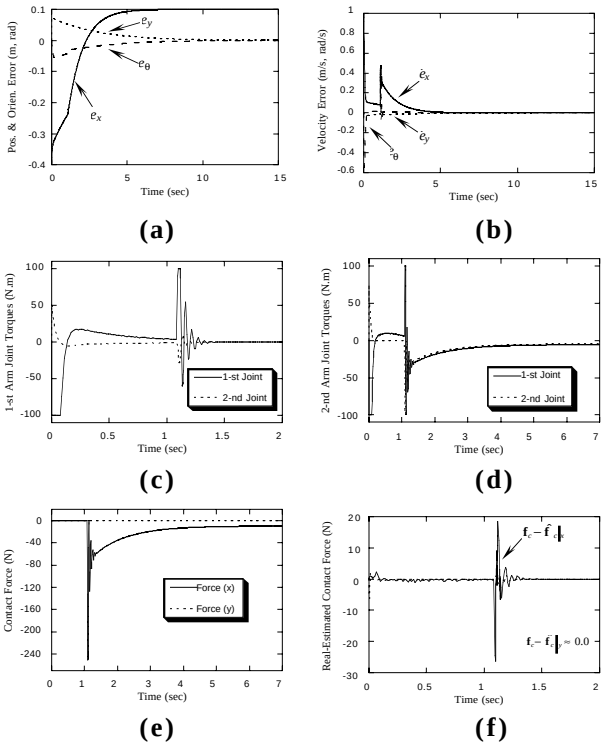

Fig. 4: Simulation results, (a) Object tracking errors, (b) Velocity errors, (c) Manipulator 1 joint torques, (d) Manipulator 2 joint torques, (e) Contact force, $\mathbf{F}_c$ (real value), (f) Difference between the real and estimated values of contact force.

A comparative analysis between existing control strategies reveals that use of a standard impedance law does not provide compensation for the object's inertia forces and yields unacceptable results when the object is massive, or when it experiences large accelerations [11]. Also, the OIC which implements the impedance law at the object level, is basically formulated for a system with rigid elements, and does not yield a good tracking in the presence of system flexibility. The more flexible the object is, the worse the performance of the OIC will be. On the other hand, as shown by simulation, performance of the MIC algorithm applied to a cooperative manipulation task is excellent,

even in the presence of flexibility, and during impact with an obstacle.

V. Conclusions.

In this paper, the new Multiple Impedance Control (MIC) was developed and applied to a space robotic system. The MIC enforces a designated impedance on cooperating manipulators *and* on the manipulated object, which results in a harmonious motion of various subsystems. Similar to the standard impedance control, one of the benefits of this algorithm is the ability to perform both free motions and contact tasks without switching the control modes. In addition, an object's inertia effects are compensated for, in the impedance law, and at the same time the end-effector(s) tracking errors are controlled. To consider the dynamic coupling between the arms and the base in space, the general MIC formulation was expanded. By error analysis it was shown that, under the MIC law, all participating manipulators, the free-flyer base, and the manipulated object exhibit the same designated impedance behavior; resulting in an adjusted tracking of various manipulators of the system together with the object. It was shown by simulation that even in the presence of flexibility and impact forces, the MIC yields a smooth and stable performance.

VI. Acknowledgments.

The support of this work by the Natural Sciences and Engineering Council of Canada (NSERC) is acknowledged. We would also like to acknowledge support of the first author from the Iran Ministry of Higher Education.

References

[1] Vafa, Z. and Dubowsky, S., “On The Dynamics of Manipulators in Space Using The Virtual Manipulator Approach,” *Proc. of IEEE Int. Conf. on Robotics and Automation*, April 1987, pp. 579-585.

[2] Umetani, Y. and Yoshida, K., “Resolved Motion Rate Control of Space Manipulators with Generalized Jacobian Matrix,” *IEEE Transactions on Robotics and Automation*, Vol. 5, No. 3, June 1989, pp. 303-314.

[3] Alexander, H. and Cannon, R., “An Extended Operational-Space Control Algorithm for Satellite Manipulators,” *The Journal of the Astronautical Sciences*, Vol. 38, No. 4, October-December 1990, pp. 473-486.

[4] Papadopoulos, E. and Dubowsky, S., “On The Nature of Control Algorithms for Free-Floating Space Manipulators,” *IEEE Transactions on Robotics and Automation*, Vol. 7, No. 6, December 1991a, pp. 750-758.

[5] Yoshida, K., Kurazume, R., and Umetani, Y., “Dual Arm Coordination in Space Free-Flying Robot,” *Proc. of IEEE Int. Conf. on Robotics and Automation*, April 1991, pp. 2516-2521.

[6] Dubowsky, S. and Papadopoulos, E., “The Dynamics and Control of Space Robotic Systems,” *IEEE Transactions on Robotics and Automation*, Vol. 9, No. 5, October 1993, pp. 531-543.

[7] Papadopoulos, E. and Moosavian, S. Ali A., "A Comparison of Motion Control Algorithms for Space Free-flyers," *Proc. of the 5th Int. Conf. on Adaptive Structures*, Sendai, Japan, December 5-7, 1994c.

[8] Hogan, N., “Impedance Control: An Approach to Manipulation -A Three Part Paper,” *ASME Journal of Dynamic Systems, Measurement, and Control*, Vol. 107, March 1985, pp. 1-24.

[9] Schneider, S. A. and Cannon, R. H., “Object Impedance Control for Cooperative Manipulation: Theory and Experimental Results,” *IEEE Transactions on Robotics and Automation*, Vol. 8, No. 3, June 1992, pp. 383-394.

[10] Meer, D. W. and Rock, S. M., “Coupled-System Stability of Flexible-Object Impedance Control,” in *Proc. of the IEEE Int. Conf. on Robotics and Automation*, Nagoya, Japan, May 1995, pp. 1839-1845.

[11] Moosavian, S. Ali A., "Dynamics and Control of Free-Flying Manipulators Capturing Space Objects," *Ph.D. thesis*, McGill University, Montreal, Canada, June 1996.

[12] Papadopoulos, E. and Moosavian, S. Ali A., “Dynamics & Control of Multi-arm Space Robots During Chase & Capture Operations,” *Proc. Int. Conf. on Intelligent Robots and Systems (IROS ‘94)*, Munich, Germany, Sept. 12-16, 1994a.

[13] Papadopoulos, E. and Moosavian, S. Ali A., “Dynamics & Control of Space Free-Flyers with Multiple Arms,” *Journal of Advanced Robotics*, Vol. 9, No. 6, 1995, pp. 603-624.

[14] Meirovitch, L., *Methods of Analytical Dynamics*, McGraw-Hill, 1970.

[15] De Fazio, T. L., Seltzer, D. S., and Whitney, D. E., “The Instrumented Remote Centre Compliance,” *Journal of The Industrial Robot*, Vol. 11, No. 4, December 1984, pp. 238-242.